The Journal of Veterinary Medical Science

NOTE

Wildlife Science

Post mortem computed tomography as a complementary tool for diagnosing cholangiohepatitis in a giant panda (*Ailuropoda melanoleuca*)

Hock Gan HENG[1,4]*, Sarah M. CHURGIN[2], Foo Khong LEE[2], Russell GRAYDON[3] and Paolo R. MARTELLI[2]

[1]Department of Veterinary Clinical Sciences, Purdue University, West Lafayette, USA
[2]Ocean Park Corporation, Hong Kong SAR, China
[3]Agriculture Fisheries and Conservation Department, Hong Kong SAR, China
[4]Present address: VetCT, Orlando, USA

J. Vet. Med. Sci.
84(7): 1010–1014, 2022
doi: 10.1292/jvms.21-0349

Received: 17 June 2021
Accepted: 12 May 2022
Advanced Epub:
26 May 2022

ABSTRACT. A geriatric female giant panda developed grave signs of illness and was diagnosed with suspected hepatobiliary tract obstruction or other severe hepatic disease such as advanced cholangiohepatitis. The giant panda was euthanized and post mortem computed tomography was performed prior to necropsy. Common bile duct obstruction at the major duodenal papilla by a mineral attenuating calculus causing dilatation of common bile and gallbladder with concurrent multiple areas of liver abscess were detected by postmortem computed tomography. These were confirmed with gross necropsy. This is the first case report of common bile duct obstruction by mineral calculus with concurrent severe cholangiohepatitis in a giant panda.

KEYWORDS: *Ailuropoda melanoleuca*, common bile duct obstruction, computed tomography, giant panda, necrotizing cholangiohepatitis

In the past few years, there is an increasing number of reports on the usage of post mortem computed tomography (PMCT) in the investigation of the cause of death in animals [8, 14]. This is especially pertinent for zoological species as there may be lack of complete history of the presentation, physical examination constraints due to large patient size or aggressive demeanor, or other challenges [2, 5, 9, 10, 13, 15, 16, 18]. It is documented that PMCT is superior to conventional necropsy in detecting fractures, as well as gas in body cavities, organ parenchyma, and the vascular system [14].

The complementary usage of PMCT to conventional necropsy in zoological species may help to increase the accuracy of conventional necropsy [7, 8, 10, 16]. The report describes obstruction of common bile duct by a mineral calculus leading to necrotizing cholangiohepatitis in a giant panda, with the clinical course, PMCT and pathological findings.

The patient was an approximately 38-year-old intact female giant panda. The panda was rescued from the wild as a 2–3-year-old juvenile in 1980 and remained under human care thereafter. Several chronic medical conditions were encountered during the panda's care including significant systemic hypertension, psychogenic polydipsia, multifocal osteoarthritis, and bilateral mature cataracts as well as lens luxation. The patient also had intermittent episodes of mucoid stool and gastrointestinal upset, as is commonly seen in captive giant pandas [12]. Long-term medications for this animal included carprofen (1–2 mg/kg p.o., s.i.d.) and amantadine (2 mg/kg p.o., s.i.d.) to address osteoarthritis, and amlodipine (0.13–0.18 mg/kg p.o., s.i.d.) to treat hypertension.

Preventative care for this patient included monthly routine blood draws for general health monitoring. Venipuncture was accomplished using operant conditioning, with the animal conscious and voluntarily participating in the procedure. About six months prior to death, routine bloodwork revealed marked elevations in liver enzymes including aspartate aminotransferase (AST, 498 µl, reference range 4–116), alanine aminotransferase (ALT, 640 µl, ref. range 23–119), and gamma-glutamyltransferase (GGT, 51 µl, ref. range 0–14) [3]. At this time total white blood cell count was within normal for this individual's in-house reference range (18.28×10^3 cells/µl, ref. range 10.44–19.3), although above range for published standards for the species ($2.41–12.43 \times 10^3$ cells/µl) [3]. Since no clinical signs were present, the patient was monitored pending a recheck of blood values. An ultrasound of the liver six days later did not reveal any abnormalities. Recheck bloodwork on day seven revealed a worsening of liver enzyme elevations

*Correspondence to: Heng, H. G.: hockganheng@yahoo.com, Department of Veterinary Clinical Sciences, Purdue University, 625, Harrison Street, West Lafayette, IN 47907, USA

(AST 623 u/l, ALT 981 µl, GGT 71 µl) and leukocytosis (26.28 × 10^3 cells/µl) characterized by a mature neutrophilia. Despite the lack of clinical signs, treatment with hepatoprotectant medications was initiated including silymarin (Legalon 70, 1 mg/kg p.o., t.i.d.) and a phospholipid supplement (Essentiale, 4 mg/kg p.o., b.i.d.). Within one week all values were improved and continued to fall until normalizing 3 months later (AST 91 µl, ALT 119 µl, GGT 15 µl). Hepatoprotectant therapy was continued for approximately five months, at which point a routine abdominal ultrasound was performed and revealed no abnormalities of the liver.

Approximately one month later, the animal developed lethargy and inappetence. Despite initial improvement over the next two days, progressive anorexia and somnolence were observed. The patient was administered non-steroidal anti-inflammatory treatment (Rimadyl, 4 mg/kg i.m.) presuming a painful condition and in view of the long-term osteoarthritis, but there was no improvement seen. On day five, the patient became severely obtunded and non-ambulatory. Bloodwork revealed profound leukocytosis (76.57 × 10^3 cells/µl) characterized by a mature neutrophilia with a mild left shift (5% bands), severe azotemia with elevations in both creatinine (9,457 mg/dl, ref. range 611–1,663 mg/dl) and urea nitrogen (20.6 mmol/l, ref. range 0.6–9.7), and severe liver enzyme elevations (AST 1,416 µl, ALT 545 µl, GGT 528 µl). Total bilirubin was also profoundly elevated (93.48 µmol/l, ref. range 0.1–4.2). These findings were supportive of hepatobiliary tract obstruction or other severe hepatic disease such as advanced cholangiohepatitis. Due to grave prognosis and multiple grave senile end-stage conditions, the patient was humanely euthanized.

Post mortem computed tomography (PMCT) (GE healthcare, Milwaukee, WI, USA) was performed about 3 hr after euthanasia. The body was placed in sternal recumbency. With a total body length of 134 cm and an abdominal girth of 116 cm, the animal easily fit into a standard CT gantry (aperture of 80 cm). Scan parameters were as follows: 140 kV; 455 mA; 0.625 mm slice thickness; matrix size of 512 × 512, and pitch of 1.

Severe abnormalities of the hepatobiliary system were detected on PMCT. There was intrahepatic linear gas throughout the hepatic parenchyma. Three focal areas of coalescing gas bubbles in the hepatic parenchyma were present. Two were at the right caudolateral aspect and one was at the right cranial aspect of the liver. There was accumulation of a small amount of fluid at the dependent aspect of the latter (Fig. 1).

The gallbladder was moderately distended and filled with dependent bile and a moderate amount of gas. The wall of the gallbladder was mildly thickened, irregular, and small intramural gas bubbles were present (Fig. 1). A large (1.32 cm), round, laminated mineral attenuating calculus was located at the major duodenal papilla. The common bile duct was dilated (1.7 cm) and filled with fluid and a small amount of gas (Fig. 2).

A very small amount of effusion was present in the cranial peritoneal cavity adjacent to the liver, and a moderate amount of effusion at the right caudal peritoneal cavity. A few gas bubbles were present in the peritoneal cavity adjacent to a few loops of intestines. There was a small mineral attenuating focus located at the left lateral wall of the caudal vena cava adjacent to the left adrenal gland. Cylindrical mineral attenuating structures were present within ventral aspect of the left adrenal gland. The right adrenal gland was normal. A few renal hypoattenuating structures were present in both kidneys (Fig. 3).

Conventional necropsy was performed the following morning, approximately 13 hr after PMCT. The mucous membranes were mildly jaundiced. The abdominal cavity contained approximately 300 ml of reddish brown, opaque fluid with fibrin. The liver was grossly abnormal with a diffuse, mottled, creamy brown to red discoloration. All liver lobes were swollen. On cut surface, bile ducts were thickened and dilated. A solitary 2.5 cm diameter creamy red abscess was present on the surface of the right central lobe, surrounded by a 1–2 mm thick band of hemorrhage. On cut surface, this lesion contained a large pocket of liquefactive necrosis. All other liver lobes contained similar but smaller foci of liquefactive necrosis. Prominent bile ducts were filled with greyish red fluid and fibrin. The gallbladder was distended, firm, and adhered tightly to the duodenum. The gallbladder wall was thickened, and the mucosal surface was lined with a creamy grey diphtheritic membrane of fibrin. Small focal hemorrhages were present under the membrane. A moderate amount of gas and approximately 50 ml of foul-smelling, grey-brown, opaque material

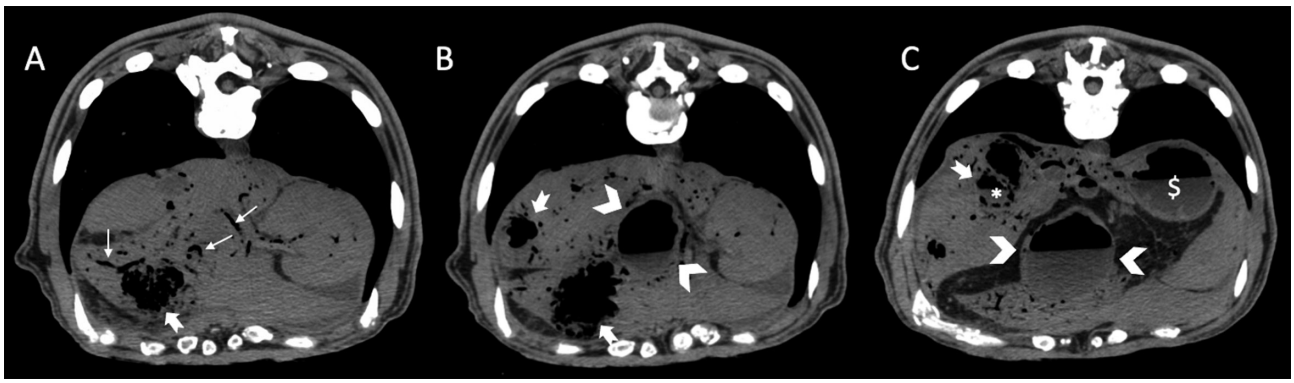

Fig. 1. Axial plane CT images of the liver, view in soft tissue window (WL: 40, WW: 350). Note the linear gas in the hepatic parenchyma (white arrows) (**A**). There were three focal areas of coalescing gas bubbles (white notched arrows) (**A** and **B**). A small amount of fluid accumulation (white asterisk) at the dependent aspect of area of coalescing gas at the right cranial dorsal aspect of the liver (**C**). Gallbladder contains gas and dependent bile, and small gas bubbles are present in the wall of the gallbladder (white chevron) (A and B). A small amount of fluid is present in the stomach (white $) (C).

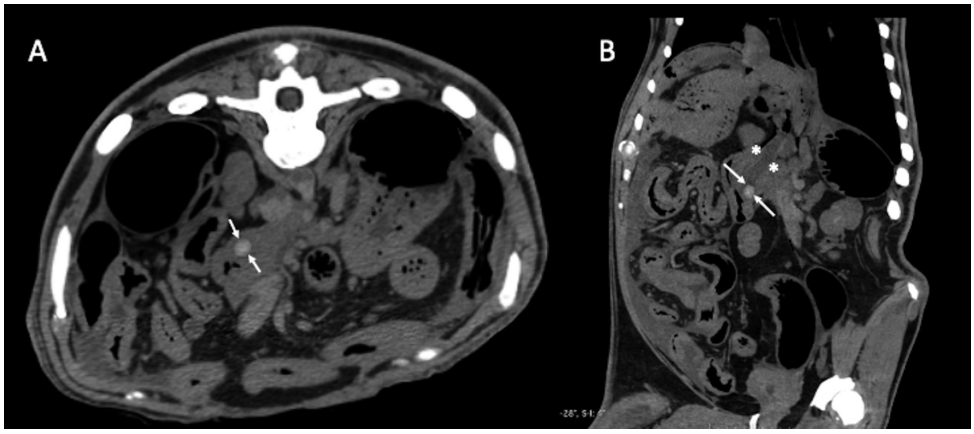

Fig. 2. Axial plane CT image (**A**) and oblique dorsal plane reconstructed CT image (**B**) view in soft tissue window (WL: 40, WW: 350). There was a large rounded laminated mineral attenuating calculus (white arrows) causing obstruction of the major duodenal papilla. Note the dilatation of the common bile duct (between white asterisks) filled with fluid and a small amount of gas.

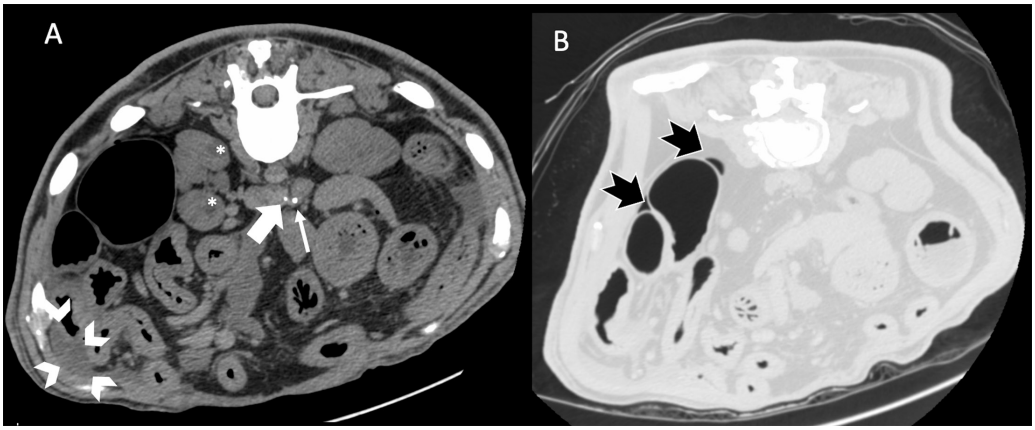

Fig. 3. **A**: Axial plain image of the abdomen in soft tissue window (WL: 40, WW: 350). A small peritoneal effusion was present in the right ventral peritoneal cavity (white chevrons), a mineral attenuation focus in the left ventral aspect of the caudal vena cava (thick white arrow), and mineral attenuating focus in the ventral aspect of the left adrenal gland (thin white arrow). Two hypoattenuating nodules in the right kidney were present (white asterisks). The margins of the kidneys are lobulated. **B**: Axial plain image of the abdomen in lung window (WL: −500, WW: 1,400). There was a small amount of gas in the peritoneal cavity (black notched arrows).

were present in the gallbladder (Fig. 3).

A round, smooth layered approximately 12 mm × 12 mm mineral calculus was present at the distal aspect of the common bile duct at the duodenal papilla (Fig. 4). The common bile duct was dilated and filled with greyish red fluid and fibrin. Mineral foci of the left adrenal gland were present. Multiple cysts in both kidneys were observed.

On histological examination, the liver showed evidence of marked post mortem decomposition. However, there was also ample evidence of severe, acute, necrotizing cholangiohepatitis with multiple variably-sized foci of necrosis and large numbers of neutrophils. There was evidence of chronic fibrosis and bile duct proliferation in the portal areas with a more acute inflammatory reaction super-imposed on the chronic changes. In many places the more acute reaction extended into the adjacent liver lobules. In one section there were numerous very large areas of necrosis with hemorrhage, fibrin, and neutrophils surrounding lytic hepatic lobules.

The gall bladder mucosa contained moderate numbers of mononuclear inflammatory cells and neutrophils. Areas of hemorrhage were present in the serosa. In a section contiguous with the liver, there was massive thickening of the wall with extensive areas of necrosis and edema, fibrin, and massive numbers of inflammatory cells. The correlation of PMCT findings with gross necropsy and pathology results is listed in Table 1.

The cause of severe illness in this animal was concluded to be partial and/or complete obstruction of the common bile duct by a choledocholith, leading to severe, necrotizing cholecystitis, cholangiohepatitis, and hepatic necrosis/abscessation. The findings of PMCT, conventional necropsy, and histology agreed with each other. The exact onset of the obstruction of the common bile duct could not be determined. The patient did have elevated liver enzymes six months prior to death, but this resolved with conservative

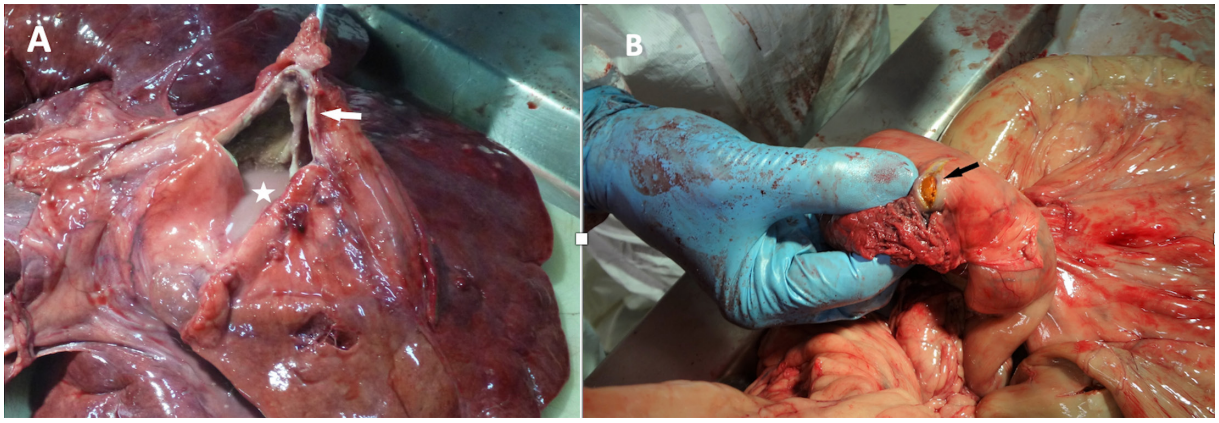

Fig. 4. **A**: The gallbladder was distended with a thickened wall (arrow) and contained abundant purulent material (star). **B**: An orange-colored choledocholith was present in the common bile duct at the level of the duodenal papilla (black arrow).

Table 1. Correlation of post mortem computed tomography findings with gross necropsy/pathology results

PMCT findings	Gross necropsy findings	Pathology/histology results
Intrahepatic linear gas		
Foci of coalescing gas bubbles in hepatic parenchyma with dependent fluid	Abscess with liquefactive necrosis	Severe, acute necrotizing cholangiohepatitis with multiple foci of necrosis and large numbers of neutrophils
Distended gallbladder with dependent bile and non-dependent gas	Distended, firm and adhered to the duodenum. Contained a moderate amount gas and 50 ml of foul smelling, grey-brown, opaque material	
Mildly thickened, irregular and intermural gas bubbles of gallbladder wall	Thickened gallbladder wall, and the mucosal surface was lined with a creamy grey diphtheritic membrane of fibrin	Massive thickening of gallbladder wall with extensive areas of necrosis and edema, fibrin, and inflammation
Layered mineral calculus at major duodenal papilla	Smooth layered mineral calculus at the duodenal papilla	
Dilated common bile duct with fluid and gas	Dilated common bile duct with greyish red fluid and fibrin	
Small amount of peritoneal effusion	Peritoneal effusion (reddish brown, opaque with fibrin)	
Small gas bubbles in the peritoneal cavity		
Mineral focus at left lateral wall of caudal vena cava		
Mineral focus at left adrenal gland	Mineral focus in left adrenal gland	
Hypoattenuating structures in both kidneys	Multiple renal cysts	

therapy (hepatoprotectant medications) and thus was unlikely to have been reflective of ongoing bile duct obstruction. The obstruction may have been intermittent or recurrent. However, there may indeed have been cholangitis or cholangiohepatitis present at the time of the live enzyme elevations, and it may have led ultimately to stone formation in the bile duct. Ultrasonographic examination of the liver at multiple points during the six-month period did not reveal obvious abnormalities. The liver may either have indeed been normal at those times, or the limitations of conscious ultrasound in this species may have precluded accurate imaging of the entire liver. The common bile duct was not examined during the ultrasound exams due to overlying gas-filled intestine and technical challenges due to the large body size patient.

In dogs, cholelithiasis is one of the more common diseases of the gall bladder, and stones can migrate to the common bile duct or form there in cases of primary choledocholithiasis [1]. Dogs may be asymptomatic or may present with signs such as icterus, abdominal pain, vomiting, and anorexia. When severe biliary obstruction occurs, surgical intervention is usually required and may be accomplished via multiple techniques, with or without placement of stents [6]. The incidence and outcome of complications of obstructive disease such as the hepatic necrosis and abscessation seen in this giant panda is unknown. Because the animal's status deteriorated rapidly after the onset of clinical signs and the condition was considered moribund, aggressive treatment such as surgery was not considered.

The severity of the pathology as demonstrated by the accumulation of gas in the hepatic parenchyma, intrahepatic bile duct and

common bile duct seen on the PMCT may be missed or underestimated by the conventional necropsy. This is because conventional necropsy may not accurately estimate the amount of gas in body cavities, organ parenchyma and vascular system, and thus the severity of disease [14]. The gas in the hepatic parenchyma, intrahepatic bile duct and common bile duct seen on the PMCT was not due to post mortem putrefaction as PMCT was performed soon after euthanasia [4, 11]. Thus, it is likely that this finding was indicative of a severe, gas-forming bacterial infection. This is also supported by the finding of necrotizing cholangiohepatitis on histopathology. Bacterial cultures of the liver yielded growth of *Enterococcus faecalis, E. coli, Morganella morganii,* and *Clostridium perfringens*. A clostridial infection could certainly have caused gas production in the organs, but it is difficult to ascertain whether this particular bacteria grew on post mortem cultures as a result of true infection vs. post mortem decomposition. The same bacterial species grew from multiple other organs sampled during the necropsy, so it is likely that the *Clostridium* was reflective of post mortem overgrowth. The underlying cause of the gas formation seen on PMCT thus is not definitively known.

To the authors' knowledge, this is the first report of both choledocholithiasis and the resulting severe hepatopathy in a giant panda. Post mortem CT is a useful adjunct to conventional necropsy [14, 17]. In this case, the PMCT was particularly helpful in identifying the calculus in the bile duct prior to conventional necropsy, leading the prosectors to delicately dissect this area in order to confirm and demonstrate the gross lesions. In zoological species, PMCT can also be useful to help elucidate the anatomy of species that are rarely presented for necropsy [10, 13, 16], and can alert the prosectors of anatomical peculiarities of the species or individual.

POTENTIAL CONFLICTS OF INTEREST. The authors have nothing to disclose.

REFERENCES

1. Aguirre, A. 2017. Diseases of the gallbladder and extrahepatic biliary system. pp. 1674–1680. In: Textbook of Veterinary Internal Medicine: Diseases of the Dog and the Cat 8th ed. (Ettinger, S. J., Feldman, E. C., Cote, E. eds.), Elsevier, St. Louis.
2. Campos Fonseca Pinto, A. C. B., Massad, M. R. D., Ribas, L. M., Baroni, C. O., Tremori, T. M., Reis, S. T. J. and Rocha, N. S. 2017. Post-mortem computed tomography angiography and forensic necropsy of a brown howler monkey: A case report. *J. Forensic Radiol. Imaging* **8**: 48–51. [CrossRef]
3. Collins, D. M. 2015. Ursidae. pp. 498–508. In: Fowler's Zoo and Wild Animal Medicine, Volume 8 (Miller, R. E. and Fowler, M. E. eds.), Elsevier, St. Louis.
4. Fischer, F., Grimm, J., Kirchhoff, C., Reiser, M. F., Graw, M. and Kirchhoff, S. 2012. Postmortem 24-h interval computed tomography findings on intrahepatic gas development and changes of liver parenchyma radiopacity. *Forensic Sci. Int.* **214**: 118–123. [Medline] [CrossRef]
5. Franckenberg, S. 2015. Fatal gunshot to a fox: the Virtopsy approach in a forensic veterinary case. *J. Forensic Radiol. Imaging* **3**: 72–75. [CrossRef]
6. Folk, C. and Lux, C. 2019. Choledochotomy for obstructive choledocholithiasis in two dogs. *Case Rep. Vet. Med.* **2019**: 4748194. [Medline]
7. Gascho, D., Hetzel, U., Schmid, N., Martinez, R. M., Thali, M. J. and Richter, H. 2020. Virtopsy of a gravid *Boa constrictor* using computed tomography and magnetic resonance imaging. *Vet. Anim. Sci.* **10**: 100150. [Medline] [CrossRef]
8. Grela, M., Panasiuk-Flak, K., Listos, P., Gryzińska, M., Buszewicz, G., Chagowksi, W. and Teresiński, G. 2020. Post-mortem analysis of gunshot wounds to the head and thorax in dogs by computed tomography, radiography and forensic necropsy. *Med. Sci. Law* **61**: 105–113. [Medline]
9. Hamano, T., Terasawa, F., Tachikawa, Y., Murai, A., Mori, T., El-Dakhly, K., Sakai, H. and Yanai, T. 2014. Squamous cell carcinoma in a capybara (Hydrochoerus hydrochaeris). *J. Vet. Med. Sci.* **76**: 1301–1304. [Medline] [CrossRef]
10. Hamel, P. E. S., Giglio, R. F., Cassle, S. E., Farina, L. L., Leone, A. M. and Walsh, M. T. 2020. Postmortem computed tomography and magnetic resonance imaging finding in a case of coinfection of dolphin morbillivirus and aspergillus fumigatus in a juvenile Bottlenose Dolphin (*Tursiops Truncatus*). *J. Zoo Wildl. Med.* **51**: 448–454. [Medline] [CrossRef]
11. Heng, H. G., Selvarajah, G. T., Lim, H. T., Ong, J. S., Lim, J. and Ooi, J. T. 2009. Serial postmortem abdominal radiographic findings in canine cadavers. *Forensic Sci. Int.* **192**: 43–47. [Medline] [CrossRef]
12. Janssen, D. L., Morris, P., Sutherland-Smith, M., Greenberg, M., Li, D., Mauroo, N. and Spelman, L. 2006. Medical management of captive adult and geriatric giant pandas. pp. 353–376. In: Giant Pandas: Biology, Veterinary Medicine and Management (Wildt, D. E., Zhang, A., Zhang, H., Janssen, D. L. and Ellis, S. eds.), University Press, Cambridge.
13. Lee, K. J., Sasaki, M., Miyauchi, A., Kishimoto, M., Shimizu, J., Iwasaki, T., Miyake, Y. and Yamada, K. 2011. Virtopsy in a red kangaroo with oral osteomyelitis. *J. Zoo Wildl. Med.* **42**: 128–130. [Medline] [CrossRef]
14. Ribas, L. M., Massad, M. R., Pinto, A. C. B. C. F., Heng, H. G., Tremori, T. M., Reis, S. T., Baroni, C. O., Massad, E. and Rocha, N. S. 2020. Post-mortem CT vs necropsy in feline medicine. *J. Feline Med. Surg.* **22**: 1206–1213. [Medline] [CrossRef]
15. Thali, M. J., Kneubuehl, B. P., Bolliger, S. A., Christe, A., Koenigsdorfer, U., Ozdoba, C., Spielvogel, E. and Dirnhofer, R. 2007. Forensic veterinary radiology: ballistic-radiological 3D computertomographic reconstruction of an illegal lynx shooting in Switzerland. *Forensic Sci. Int.* **171**: 63–66. [Medline] [CrossRef]
16. Weisbrod, T. C., Walsh, M. T., Marquardt, S. and Giglio, R. F. 2020. Computed tomography diagnosis of pneumothorax and cardiac foreign body secondary to stingray injury in a Bottlenose Dolphin (*Tursiops truncatus*). *Aquat. Mamm.* **46**: 326–330. [CrossRef]
17. Yamada, K., Toyotome, T., Matsumoto, N. and Itoh, M. 2020. Autopsy imaging for aspergillosis in King Penguin, an economically valuable zoo animal. *J. Vet. Med. Sci.* **82**: 373–375. [Medline] [CrossRef]
18. Zürcher-Giovannini, S., Ruder, T. D., Pool, R., Erdelyi, K. and Origgi, F. C. 2020. Mandibular ossifying fibroma and multiple oral papillomas in a Roe Deer (*Capreolus capreolus*). *Front. Vet. Sci.* **7**: 166. [Medline] [CrossRef]